

Kelvin-Helmholtz instabilities across periodic plates

By Tom Chou

Dept. of Biomathematics and Dept. of Mathematics, UCLA, Los Angeles, CA 90095-1766 USA

(Received 15 July 2018)

We consider the linear stability of two inviscid fluids, in the presence of gravity, sheared past each other and separated by an flexible plate. Conditions for exponential growth of velocity perturbations are found as functions of the flexural rigidity of the plate and the shear rate. This Kelvin-Helmholtz instability is then analysed in the presence of plates with spatially periodic (with period a) flexural rigidity arising from, for example, a periodic material variation. The eigenvalues of this periodic system are computed using Bloch's Theorem (Floquet Theory) that imposes specific Fourier decompositions of the velocity potential and plate deformations. We derive the nonhermitian matrix whose eigenvalues determine the dispersion relation. Our dispersion relation shows that plate periodicity generally destabilises the flow, compared to a uniform plate with the same mean flexural rigidity. However, enhanced destabilisation and stabilization can occur for disturbances with wavelengths near an even multiple of the plate periodicity. The sensitivity of flows with such wavelengths arises from the nonpropagating, "Bragg reflected" modes coupled to the plate periodicity through the boundary condition at the plate.

1. Introduction

When two immiscible fluids are sheared relative to each other, the flow, and the normally flat interface between them, may become unstable. This classical Kelvin-Helmholtz instability (Chandrasekar (1961), Drazin & Reid (2004), Whitham (1999)) arises from perturbations of the fluid velocity that grows into a vortex sheet due to local Bernoulli variations in pressure. The presence of gravity also tunes this instability, depending on the mass density difference and shear rate between the two fluids. If the denser fluid is in lower gravitational potential, there is a critical shear rate beyond which small perturbations grow exponentially. This instability first arises in modes of the fluid velocity perturbation that have wavevectors greater than a critical wavevector. All velocity perturbations with sufficiently small wavelength become unstable as long as the shear rate exceeds a critical value. However, very small wavelength perturbations can be stabilised if additional restoring forces from, say, an interfacial surface tension (Whitham (1999)), or a separating elastic plate are included. The Kelvin-Helmholtz instability, and its generalisations, have been thoroughly studied, for example, in the context of knotting in astrophysical jets (Blanford & Rees (1974)), cloud top entrainment instabilities (Reiss & Corona (1977)), magneto-hydrodynamic instabilities (Chandrasekar (1961) and Frank *et al.* (1996)), and the flutter of panels (Miles (1956)).

In the context of potential applications involving fluid-structure interactions, we consider the Kelvin-Helmholtz instability in the presence of an infinitesimally thin bendable plate separating the two inviscid flows, as shown in Figure 1. We assume the plate is

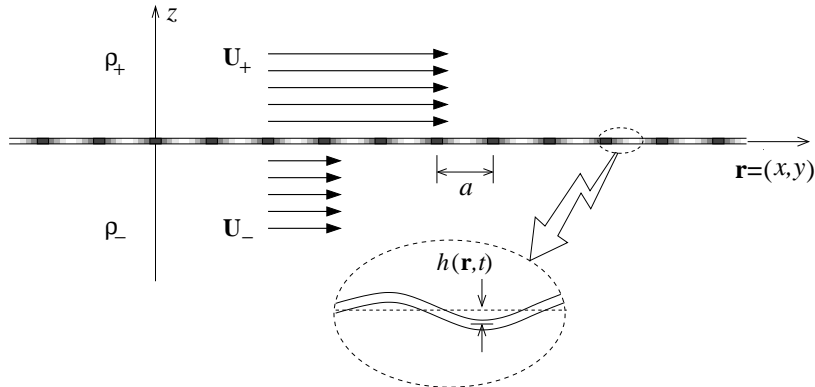


FIGURE 1. Discontinuous shear flow separated by a periodically flexible plate.

thin and inextensible, such that only bending modes can be excited. Since elastic restoring forces stabilize short wavelength perturbations, instabilities arise only for perturbations that have wavevectors within a certain window of values. Furthermore, we consider an elastic membrane that has spatially periodic properties, such as mass density or bending rigidity, which might arise, for example, in an engineered composite structure. By itself (in the absence of fluid), a periodic plate supports stable bending waves that propagate *except* at band gaps, *i.e.* frequencies corresponding to waves that have half-integer wavelengths in one period of the structural variation (Ashcroft & Mermin (1976) and Joannopolous, Meade, & Winn (1995)). Waves near these wavelengths have vanishing group velocities and do not propagate in an infinite periodic medium due to their multiple “Bragg” reflections and destructive interference. Properties of wave propagation through periodic media have been computed in numerous physical settings, including acoustic waves moving through materials with periodic sound speeds (Sigalas & Economou (1992)), electromagnetic propagation through periodic dielectrics (Joannopolous, Meade, & Winn (1995)), and water wave propagation over periodic structures (Chen *et al.* (2004), Chou (1998), Hu & Chan (2005), Hu *et al.* (2003), Naciri & Mei (1988), Peter, Meylan, & Linton (2006), Porter & Evans (1996)).

In this paper, we combine the periodic stabilizing membrane with an otherwise unstable shear flow and study the complex dispersion relation. A velocity perturbation with any wavevector, convected by the base laminar flow forms a travelling wave. This travelling wave, when coupled to the intrinsic periodicity of the elastic plate may be Bragg reflected and not able to propagate within the region of periodicity, altering its stability characteristics. In order to explore this heuristic argument further, we formulate in the next section the linear problem in terms of a vorticity-free velocity perturbation and a small deformation of the separating elastic membrane. We review, in turn, a uniform plate subject to destabilizing flow, and a free periodic plate that supports stable waves. The fully coupled problem, a periodic plate in destabilising flow, is then presented in the Results section. We show that the stability properties are affected most when the wavelengths of the most unstable modes are close to the periodicity of the plate flexibility. Implications and extensions to related flow systems are discussed the Discussion and Conclusions.

2. Linear Model

Consider the fluid-structure interaction depicted in Figure 1. Two incompressible fluids flowing uniformly in two different directions, \mathbf{U}_+ and \mathbf{U}_- , in the $x-y$ plane are separated by a negligibly thin elastic plate. Gravitational acceleration is in the $-\mathbf{z}$ direction. Since viscosity will be neglected, we will consider only potential flows. The total velocity in each region (\pm) is defined by the uniform flow \mathbf{U}_\pm plus a small irrotational perturbation $\mathbf{v}_\pm \equiv \nabla\varphi_\pm$. Upon imposing incompressibility, the upper and lower velocity potentials, φ_\pm , satisfy Laplace's equation:

$$(\nabla_\perp^2 + \partial_z^2)\varphi_\pm(\mathbf{r}, z, t) = 0, \quad \nabla_\perp^2 = \partial_x^2 + \partial_y^2. \quad (2.1)$$

Since $\partial_z\varphi|_{z=0} \approx v_z$ is the vertical velocity of the surface, the kinematic conditions at the plate-separated interface are

$$\partial_t h(\mathbf{r}, t) + \mathbf{U}_\pm \cdot \nabla_\perp h(\mathbf{r}, t) - \lim_{\varepsilon \rightarrow 0} \partial_z \varphi_\pm(\mathbf{r}, \pm\varepsilon, t) = 0, \quad (2.2)$$

where $h(\mathbf{r}, t)$ is the normal displacement of the plate. The linearized normal stress balance at the interface, including the normal forces arising from the flexible plate, is

$$[\rho\dot{\varphi} + \rho\mathbf{U} \cdot \nabla_\perp \varphi + \rho gh(\mathbf{r}, t)]_\pm^+ = m(\mathbf{r})\ddot{h}(\mathbf{r}, t) + \nabla_\perp^2 (D(\mathbf{r})\nabla_\perp^2 h(\mathbf{r}, t)), \quad (2.3)$$

where $[X]_\pm^+ \equiv \lim_{\varepsilon \rightarrow 0} X(z = \varepsilon) - X(z = -\varepsilon)$. In Eq. 2.3, $m(\mathbf{r})$ and $D(\mathbf{r})$ are the mass per unit area and the flexural rigidity of the plate, respectively. Since $h(\mathbf{r}, t)$ and $\varphi(\mathbf{r}, z, t)$ are defined only up to a constant, we need only consider the nonzero wavevector decompositions of the plate displacement and velocity potential,

$$h(\mathbf{r}, t) = \sum_{\mathbf{q} \neq 0} \int h_{\mathbf{q}}(\omega) e^{i\mathbf{q} \cdot \mathbf{r} - i\omega t} \frac{d\omega}{2\pi} \quad \text{and} \quad \varphi_\pm(\mathbf{r}, z, t) = \sum_{\mathbf{q} \neq 0} \int \varphi_{\mathbf{q}}^\pm(\omega) e^{i\mathbf{q} \cdot \mathbf{r} - i\omega t \mp |\mathbf{G} - \mathbf{q}|z} \frac{d\omega}{2\pi}. \quad (2.4)$$

In Eqs. 2.4, we have also assumed a continuous time-harmonic decomposition. The representation of $\varphi_\pm(\mathbf{r}, z, t)$ automatically satisfies Eq. 2.1 and the boundary conditions at $z \rightarrow \pm\infty$.

The periodic plate mass density and rigidity functions that obey $m(\mathbf{r}) = m(\mathbf{r} + \mathbf{R})$ and $D(\mathbf{r}) = D(\mathbf{r} + \mathbf{R})$, where $\mathbf{R} = n_1 a_1 \mathbf{e}_1 + n_2 a_2 \mathbf{e}_2$ (n_1, n_2 integers) is any basis vector describing the periodicity. Here, a_1, a_2 are the periodicities of $m(\mathbf{r})$ and $D(\mathbf{r})$ in the $\mathbf{e}_1, \mathbf{e}_2$ directions. The periodic functions $m(\mathbf{r})$ and $D(\mathbf{r})$ can thus be decomposed into a Fourier sum over reciprocal lattice vectors \mathbf{G} ,

$$m(\mathbf{r}) = \sum_{\mathbf{G}} m(\mathbf{G}) e^{i\mathbf{G} \cdot \mathbf{r}} \quad \text{and} \quad D(\mathbf{r}) = \sum_{\mathbf{G}} D(\mathbf{G}) e^{i\mathbf{G} \cdot \mathbf{r}}. \quad (2.5)$$

The reciprocal lattice vectors $\mathbf{G} = n_1 \mathbf{G}_1 + n_2 \mathbf{G}_2$ are defined by the reciprocal lattice basis vectors

$$\mathbf{G}_1 = \frac{2\pi}{a_1} \frac{\mathbf{e}_2 \times \mathbf{z}}{\mathbf{e}_1 \cdot (\mathbf{e}_2 \times \mathbf{z})} \quad \text{and} \quad \mathbf{G}_2 = \frac{2\pi}{a_2} \frac{\mathbf{z} \times \mathbf{e}_1}{\mathbf{e}_1 \cdot (\mathbf{e}_2 \times \mathbf{z})}. \quad (2.6)$$

Finally, we assume a large plate with dimensions $L_1 \times L_2$ that fit an integer multiple of the period ($L_1 = N_1 a_1$ and $L_2 = N_2 a_2$) and impose periodic boundary conditions on the entire system: $m(\mathbf{r} + N_i a_i \mathbf{e}_i) = m(\mathbf{r})$ and $D(\mathbf{r} + N_i a_i \mathbf{e}_i) = D(\mathbf{r})$ for $i = 1, 2$. Under this construction, the wavevector sum in the decompositions 2.4 are taken over

$\mathbf{q} = \sum_{n_i \neq 0} (n_i/N_i) \mathbf{G}_i$. In the $L_1, L_2 \rightarrow \infty$ limit, sums over \mathbf{q} become the Cauchy principle value of the corresponding Riemann integral.

After substitution of Eqs. 2.4 into the kinematic conditions 2.2, we find the relationship

$$\varphi_{\mathbf{q}}^{\pm}(\omega) = \pm \frac{i(\omega - \mathbf{U}_{\pm} \cdot \mathbf{q})}{|\mathbf{q}|} h_{\mathbf{q}}(\omega), \quad \mathbf{q} \neq 0. \quad (2.7)$$

Upon substitution of Eqs. 2.4, 2.5, and 2.7 into Eq. 2.3, and exploiting the orthogonality of the $e^{i\mathbf{q} \cdot \mathbf{r}}$ basis functions,

$$\begin{aligned} & [(\rho_+ + \rho_-)\omega^2 - 2\omega(\rho_+ \mathbf{U}_+ + \rho_- \mathbf{U}_-) \cdot \mathbf{q} + \rho_+(\mathbf{q} \cdot \mathbf{U}_+)^2 + \rho_-(\mathbf{q} \cdot \mathbf{U}_-)^2 + (\rho_+ - \rho_-)g|\mathbf{q}|] h_{\mathbf{q}} \\ & = -\omega^2 |\mathbf{q}| \sum_{\mathbf{G}'} m(\mathbf{G}') h_{\mathbf{q}-\mathbf{G}'} + \sum_{\mathbf{G}'} |\mathbf{q}|^3 |\mathbf{q} - \mathbf{G}'|^2 D(\mathbf{G}') h_{\mathbf{q}-\mathbf{G}'}. \end{aligned} \quad (2.8)$$

Equation 2.8 shows that each coefficient $h_{\mathbf{q}}$ is linked with $N_1 \times N_2$ other coefficients $h_{\mathbf{q}-\mathbf{G}'}$. This problem can be solved numerically by truncating $h_{\mathbf{q}-\mathbf{G}'} \approx 0$ for large $|\mathbf{G}'|$ where $m(\mathbf{G})$ and $D(\mathbf{G})$ are small. Alternatively, Eq. 2.8 can be organized according to the ‘‘reduced zone scheme,’’ by defining $\mathbf{k} = \mathbf{q} - \mathbf{G}$, where \mathbf{G} is such that \mathbf{k} is restricted in the first Brillouin zone defined by $|\mathbf{k} \cdot \mathbf{e}_i| < |\mathbf{G}_i \cdot \mathbf{e}_i|/2$ (Ashcroft & Mermin (1976)). In this representation, we need only consider the $N_1 \times N_2$ eigenvalues, each with index \mathbf{k} inside the first Brillouin zone. The problem is thus cast into a quadratic eigenvalue problem defined by

$$\sum_{\mathbf{G}'} [A_{\mathbf{k}}(\mathbf{G}, \mathbf{G}')\omega^2 + B_{\mathbf{k}}(\mathbf{G}, \mathbf{G}')\omega + C_{\mathbf{k}}(\mathbf{G}, \mathbf{G}')] h_{\mathbf{k}-\mathbf{G}'}(\omega) = 0, \quad (2.9)$$

where

$$\begin{aligned} A_{\mathbf{k}}(\mathbf{G}, \mathbf{G}') &= \frac{\rho_+ + \rho_-}{|\mathbf{k} - \mathbf{G}|} \delta_{\mathbf{G}, \mathbf{G}'} + m(\mathbf{G}' - \mathbf{G}) \\ B_{\mathbf{k}}(\mathbf{G}, \mathbf{G}') &= -2 \left[\rho_+ \frac{\mathbf{U}_+ \cdot (\mathbf{k} - \mathbf{G})}{|\mathbf{k} - \mathbf{G}|} + \rho_- \frac{\mathbf{U}_- \cdot (\mathbf{k} - \mathbf{G})}{|\mathbf{k} - \mathbf{G}|} \right] \delta_{\mathbf{G}, \mathbf{G}'} \\ C_{\mathbf{k}}(\mathbf{G}, \mathbf{G}') &= \left[\rho_+ \frac{(\mathbf{U}_+ \cdot (\mathbf{k} - \mathbf{G}))^2}{|\mathbf{k} - \mathbf{G}|} + \rho_- \frac{(\mathbf{U}_- \cdot (\mathbf{k} - \mathbf{G}))^2}{|\mathbf{k} - \mathbf{G}|} + (\rho_+ - \rho_-)g \right] \delta_{\mathbf{G}, \mathbf{G}'} \\ &\quad - |\mathbf{k} - \mathbf{G}|^2 |\mathbf{k} - \mathbf{G}'|^2 D(\mathbf{G}' - \mathbf{G}). \end{aligned} \quad (2.10)$$

Equation 2.9 is a matrix equation for $h_{\mathbf{k}-\mathbf{G}}(\omega)$ that has solutions for only certain $\omega(\mathbf{k})$. The full dispersion relation can be recovered by assigning the appropriate translation \mathbf{G} in the eigenvalues $\omega(\mathbf{k} - \mathbf{G})$ to $\omega(\mathbf{q})$ for wavevectors \mathbf{q} outside the first Brillouin zone. The system becomes unstable when $\omega(\mathbf{q})$ acquires an imaginary component.

In anticipation of a length scale a associated with the periodicity in the plate properties, we henceforth nondimensionalise all parameters and eliminate ρ_-, g and a according to

$$\begin{aligned} \mathbf{r} &\rightarrow \mathbf{r}/a, \quad \mathbf{G} \rightarrow a\mathbf{G}, \quad \mathbf{k} \rightarrow a\mathbf{k}, \quad \omega \rightarrow \sqrt{\frac{a}{g}}\omega, \quad \mathbf{U}_{\pm} \rightarrow \frac{\mathbf{U}_{\pm}}{\sqrt{ag}} \\ D &\rightarrow \frac{D}{a^4 \rho_- g}, \quad m \rightarrow \frac{m}{a \rho_-}, \quad \text{and } h_{\mathbf{k}}(\mathbf{G}) \rightarrow h_{\mathbf{k}}(\mathbf{G})/a. \end{aligned} \quad (2.11)$$

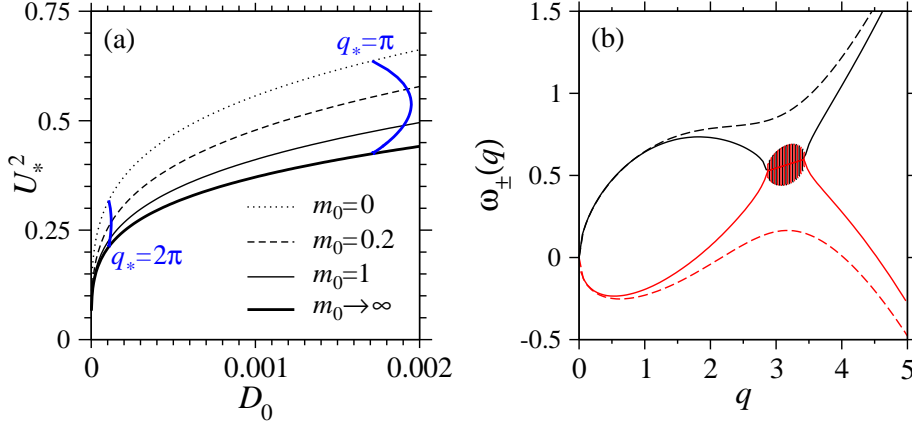


FIGURE 2. (a) The curve relating the critical value of the shear U_* to the constant flexural rigidity D_0 , for various values of the uniform plate mass density m_0 . For velocities greater than U_* , the flow becomes unstable. For different plate mass densities, the sets of D_* , U_* that give rise to an initial instability at wavevectors $q_* = \pi$ and $q_* = 2\pi$ are shown by the black arcs spanning the curves. (b) The dispersion relation for a uniform plate just after the onset of instability.

2.1. A Uniform Plate in the Presence of Flow

First consider the standard Kelvin-Helmholtz instability in the presence of a uniform elastic plate, where $m = m_0$ and $D(\mathbf{r}) = D_0$ are constants. Miles (2001) treated a similar problem of a thin boundary layer over an elastic plate. Since $D(\mathbf{G}) = D_0 \delta_{\mathbf{G},0}$ and $m(\mathbf{G}) = m_0 \delta_{\mathbf{G},0}$, Eq. 2.9 is diagonal and is satisfied when

$$\Gamma(q)\omega_{\pm}(\mathbf{q}) = (\gamma \mathbf{U}_+ + \mathbf{U}_-) \cdot \mathbf{q} \pm \sqrt{\Delta(\mathbf{q})}, \quad (2.12)$$

where $\Gamma(q) \equiv \gamma + 1 + m_0 q$, and the discriminant

$$\Delta(\mathbf{q}) \equiv \Gamma(q)(D_0 q^5 + (1 - \gamma)q) - \gamma((\mathbf{U}_+ - \mathbf{U}_-) \cdot \mathbf{q})^2 - m_0 q(\gamma(\mathbf{U}_+ \cdot \mathbf{q})^2 + (\mathbf{U}_- \cdot \mathbf{q})^2). \quad (2.13)$$

The eigenvalues ω_{\pm} become complex when $\Delta(\mathbf{q})$ becomes negative, leading to exponentially growing perturbations. In the limit where the influence of the plate is negligible ($m_0, D_0 \approx 0$) the dispersion relation reduces to that of the standard Kelvin-Helmholtz instability. The inclusion of membrane stiffness ($D_0 > 0$) tends to stabilise small wavelength modes. For any given $m_0 \geq 0$, the pairs of critical D_0 and U (denoted D_* and U_*) that give the onset of instability at a chosen wavevector q_* can be expressed explicitly in two flow configurations where \mathbf{U}_{\pm} and the \mathbf{q} corresponding to the most unstable velocity perturbations are all collinear. When \mathbf{U}_{\pm} are collinear, the onset of instability arises when $\Delta(\mathbf{q}) = 0$ is solved by two critical repeated, real roots, q_* , in addition to the root at $q = 0$ and two complex conjugate roots. For a static configuration of the lower fluid ($\mathbf{U}_- = 0$ in the reference frame of the plate), we find

$$\begin{aligned} D_* &= \frac{(1 + m_0 q_*)^2 - \gamma^2(1 + 2m_0 q_*) - \gamma m_0^2 q_*^2}{q_*^4(3(1 + \gamma + m_0^2 q_*^2) + 2(\gamma + 3)m_0 q_*)} \\ U_*^2 &= \frac{4(1 - \gamma)(1 + \gamma + m_0 q_*)^2}{\gamma q_* (3(1 + \gamma + m_0^2 q_*^2) + 2(\gamma + 3)m_0 q_*)}. \end{aligned} \quad (2.14)$$

Alternatively, for a chosen value of D_0 , the critical U_* and the corresponding initially

unstable wavevector can be found implicitly. The critical velocities U_* , as a function of D_0 and m_0 are shown in Fig. 2(a). Note that the critical velocity U_* decreases as the plate mass density m_0 increases. The limit $m_0 \rightarrow \infty$ is different from the $\rho_{\pm} \rightarrow 0$ limit treated in the next section. Here, the plate flexibility remains constant as its mass density increases. Although the magnitude of $\omega_{\pm}(q)$ decreases, the discriminant (Eq. 2.13) becomes negative at smaller U_* due to the increased inertial forces of the plate back on the fluid.

The two branches of the full dispersion relation $\omega_{\pm}(q)$ are plotted in Fig. 2(b). We have chosen parameters ($D_*(\pi)$ and U_*^2 defined by Eqs. 2.14) such that the onset of instability arises at $q_* \approx \pi$. For $U = 1/\sqrt{2} < U_*(q_* = \pi) = 0.756320$, $\omega_{\pm}(q)$ are real, as shown by the dashed curves. We also plot (solid curves) the dispersion relation for $U = 0.761577 > U_*(q_* = \pi) = 0.75632$, whereupon a window of instability opens near $q_* = \pi$. The magnitude of the complex parts of $\omega_{\pm}(q)$ are indicated by the height of the shaded region.

In the second flow configuration, we assume a vanishing net momentum in the reference frame of the plate: $\mathbf{U}_- = -\gamma\mathbf{U}_+$. In this case, we find independent of m_0 ,

$$D_* = \frac{1-\gamma}{3q_*^4} \quad \text{and} \quad U_*^2 = \frac{4(1-\gamma)}{3\gamma(\gamma+1)q_*}, \quad (2.15)$$

and the symmetry $\omega_+(q) = -\omega_-(q)$. For $D_0 \lesssim D_*$ and/or $U \gtrsim U_*$, as defined by Eq. 2.14 or Eq. 2.15, $\omega(q \approx q_*)$ becomes complex and instability arises for a small window of wavevectors near q_* .

2.2. Dispersion Relation for a Free Periodic Plate

Now consider the limit of an isolated (but periodically structured) plate where the inertia of the bounding fluid is negligible. If the plate were uniform, the dispersion relation in the limit $\rho_{\pm} \rightarrow 0$ is simply $m_0\omega^2 = D_0q^4$. For a periodically structured plate ($m(\mathbf{G} \neq 0) \neq 0, D(\mathbf{G} \neq 0) \neq 0$), the dispersion relation can be found from Eq. 2.9 with the simplified matrices $A(\mathbf{G} - \mathbf{G}') = m(\mathbf{G} - \mathbf{G}')$, $B(\mathbf{G} - \mathbf{G}') = 0$, and $C(\mathbf{G} - \mathbf{G}') = -|\mathbf{k} + \mathbf{G}|^2|\mathbf{k} + \mathbf{G}'|^2D(\mathbf{G} - \mathbf{G}')$. Henceforth, we assume the periodicities in the plate to be sinusoidal in the \mathbf{x} -direction and take the forms

$$m(\mathbf{r}) = m_0 + 2m_1 \cos 2\pi x; \quad D(\mathbf{r}) = D_0 + 2D_1 \cos 2\pi x, \quad (2.16)$$

Although the mean mass density and bending rigidity are unchanged from m_0 and D_0 , respectively, the variations m_1 and/or D_1 will change the dispersion relation. Specifically, periodic variations will break the dispersion relation at wavevectors corresponding to waves that cannot propagate through an infinite, periodic medium. At each of these wavevectors (the ‘‘Bragg planes’’), the waves (half-integers of which fit into a period) become standing. Corresponding to these nonpropagating waves are gaps in the frequency (band gaps, or stop bands) within which an infinitely periodic material cannot be excited.

Figures 3a,b show the dispersion relation of an isolated plate with periodicities in the bending rigidity (a), and mass density (b). The frequency gaps increase as the contrast m_1 or D_1 is increased. From consideration of the eigenvectors, the standing modes near the band gaps can be shown to have either nodes or antinodes over the high flexural rigidity (or high mass density) regions, depending on which side of the band gap the wavevector q lies. These behaviour generally arise in wave propagation through periodic media. When the plate is coupled to flow, it will be the near equal-wavelength modes immediately straddling the band gaps, with different frequencies and $\sim 90^\circ$ out-of-phase, that will qualitatively affect the stability near the band gaps.

[h!]

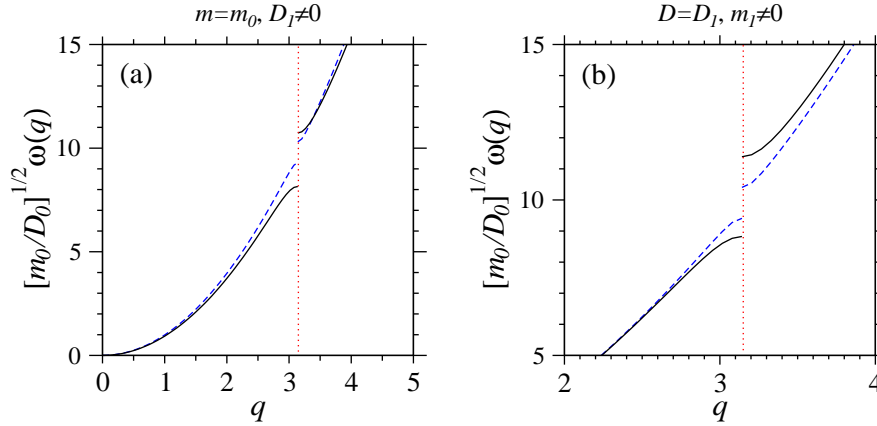


FIGURE 3. (a) The normalized dispersion relation $\sqrt{m_0/D_0} \omega_{\pm}(q)$ for $m_1 = 0$, $D_1/D_0 = 0.1$ (dashed curve) and $D_1/D_0 = 0.25$ (solid curve). (b) A blow-up of the dispersion relation for $D_1 = 0$, $m_1/m_0 = 0.1$ (dashed curve) and $m_1/m_0 = 0.25$ (solid curve).

3. Results for the Coupled Problem

We now combine the known results of the previous sections and consider the fully coupled problem where fluid instabilities and Bragg reflection interact. For simplicity, we consider the plate periodicity wavevectors ($\mathbf{G} = 2\pi n/a\mathbf{x}$) and the uniform flows $\mathbf{U}_{\pm} = U_{\pm}\mathbf{x}$ to be aligned. In the full problem, the dispersion relation $\omega(q)$ may be both complex (signalling regions of instability) and discontinuous at band gaps where $(\partial\omega/\partial q) = 0$. The full dispersion relation is found from solving the quadratic eigenvalue problem given by Eq. 2.9. This problem can be expressed in linear eigenvalue form,

$$(\mathbf{M} - \omega\mathbf{I}) \cdot \boldsymbol{\eta} = 0, \quad (3.1)$$

with $\boldsymbol{\eta} = (h_{\mathbf{k}}, \omega h_{\mathbf{k}})^T$, and

$$\mathbf{M} = \begin{pmatrix} \mathbf{0} & \mathbf{I} \\ -\mathbf{A}^{-1}\mathbf{C} & -\mathbf{A}^{-1}\mathbf{B} \end{pmatrix}. \quad (3.2)$$

The dispersion relation $\omega(\mathbf{k})$ is found from the eigenvalues of the nonhermitian matrix \mathbf{M} . For the parameters explored, we find numerical convergence of the lowest handful of eigenvalues with 40 or fewer modes \mathbf{G}, \mathbf{G}' . Therefore, we truncate the system at approximately 60 modes (where \mathbf{M} is a 120×120 matrix). This is more than sufficient to obtain numerical accuracy for the lower eigenvalues at all relevant wavevectors. The eigenvalues of \mathbf{M} are sorted from the numerical solutions and replotted in the extended zone scheme where the wavevector $0 \leq |\mathbf{q}| < \infty$. When unfolding the eigenvalues $\omega(\mathbf{k})$, we make use of the fact the functions $\omega(0 \leq |\mathbf{q}| < \infty)$ in the normal extended zone scheme come in pairs $\omega_{\pm}(\mathbf{q})$ and have the symmetry property $\omega_{\pm}(-|\mathbf{q}|) = -\omega_{\mp}(|\mathbf{q}|)$. This property, along with the consideration of the corresponding eigenvectors at each wavevector k allows us to reconstruct $\omega_{\pm}(q)$ from $\omega_{\pm}(k)$.

In Figures 4(a-c) we show the effects of increasing the strength of the periodic rigidity D_1/D_0 for the case $\mathbf{U}_{-} = 0$. In Fig. 4(a) we show a system with an incipient instability at $q \approx q_* = \pi/2$. As D_1 is increased (Figs. 4(b-c)) the bubble of instability grows modestly, while gaps in the dispersion relation also appear. The destabilising effect of rigidities

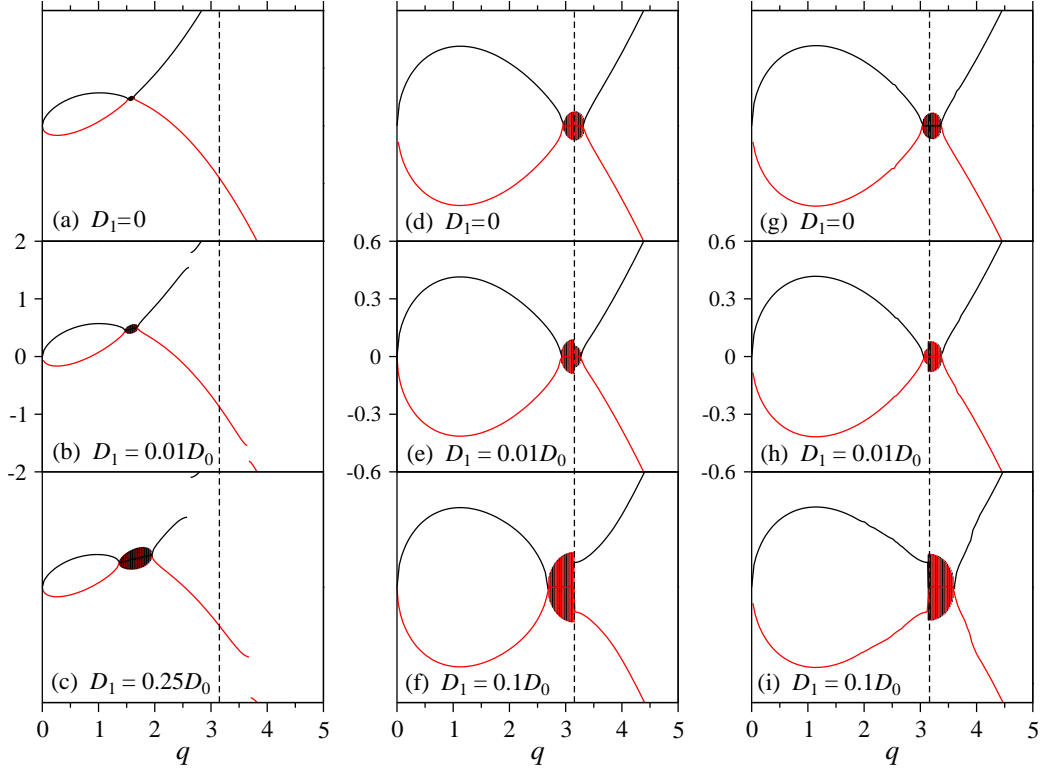


FIGURE 4. (a-c) The complex dispersion relation for a system just above the instability threshold. The instability is first triggered at $q_* = \pi/2$ (which arises for parameters $\gamma = 1/2, m_0 = 0.2, D_0 \leq D_* = 0.0298349$, and $U^2 \geq U_*^2 = 1.19809$). As D_1 increases, the instability bubble ($\text{Im}\{\omega_{\pm}\}$) increases in size as more wavevectors become unstable. (d-f) Dispersion relation for instabilities that first arise at $q_* = 3.14 \lesssim \pi$. As D_1 is increased, the modes with $q < \pi$ are destabilised, while those with $q > \pi$ are stabilised. (g-i) Increasing D_1 when the incipient instability starts at $q_* = 3.25 > \pi$ destabilises modes with $q > \pi$ and stabilises those with $q < \pi$.

with periodicity $a \gg 2\pi/q_*$ can be understood in terms of a slight effective softening of the plate to bending modes with wavelengths greater than $a\ddagger$.

Note that the gaps here do not appear at the Brillouin zone edge $q = \pi$ defined by a system's static periodic structure as in the free plate problem (Figs. 3) and in most other settings. Rather, they appear symmetrically around the band edge due to a doppler shift arising from the nonvanishing net momentum of the system. Gaps occurring away from the zone boundaries have been shown by Bermel & Warner (2002) to arise in electromagnetic propagation through deformed cholesteric elastomers.

Now consider an incipient instability that arises at higher wavevectors, near the first band gap at $q = \pi$. Assume for simplicity, the zero net momentum ($\mathbf{U}_- = -\gamma\mathbf{U}_+$) case where $\mathbf{B}_\mathbf{k}(\mathbf{G}, \mathbf{G}') = 0$ in Eq. 2.9 and $\omega_{\pm}(q) = -\omega_{\mp}(q)$. Figures 4(d-f) show the effects of increasing D_1 when the initial instability starts at $q_* = 3.14 \lesssim \pi$. As the plate heterogeneity is increased, modes with wavevector $q < \pi$ are destabilised, while those with $q > \pi$ are stabilised. Conversely, if the incipient instability arises at $q_* \gtrsim \pi$,

\ddagger The effective long wavelength bending rigidity of a plate made from alternating equal strips of two materials with individual rigidities $D_0 \pm \Delta D$ is $D_{eff} = 2/(1/(D_0 + \Delta D) + 1/(D_0 - \Delta D)) \approx D_0 - (\Delta D)^2/D_0$

as in Figs. 4(g-i) (where $q_* = 3.25$), increasing D_1 will destabilise modes with $q > \pi$, while stabilising those with $q < \pi$. The discontinuous change in the eigenvalues across the Bragg plane $q = \pi$ occurs first in the imaginary component and the growth rate $\text{Im}\{\omega(q)\}$ is discontinuous. As the contrast D_1/D_0 is further increased, $\text{Re}\{\omega(q)\}$ also becomes discontinuous. This behavior can be explicitly seen with perturbation analysis of Eq. 3.2 by truncating the matrix and finding the four eigenvalues as $q \rightarrow \pi$.

4. Discussion and Conclusions

We have analysed the properties of the instabilities of two fluids uniformly flowing past each other, separated by an elastic plate with periodic bending rigidity and/or mass density. Our generalization of the Kelvin-Helmholtz instability can be quantified by finding the eigenvalues and eigenvectors of a nonhermitian matrix (Eq. 2.9). The imaginary components of the eigenvalues $\omega(q)$ determine the rate of unstable growth for eigenmodes of wavevector q . We find that an imposed plate periodicity generally destabilises the flow but that the destabilisation mainly occurs in the band of wavevectors on the side of the initially most unstable mode. Modes with wavevectors on the other side of the band gap from the most unstable wavevector q_* are stabilised as D_1 is increased.

The destabilisation/stabilisation that occurs on either side of the band gap can be understood in terms of $\sim 90^\circ$ out-of-phase standing modes with wavevectors $q = (2n - 1)\pi \pm \varepsilon$ immediately straddling the n^{th} band gap. For example, if $q_* \gtrsim (2n - 1)\pi$, increasing D_1 destabilises the waves with $q \approx q_*$ since their antinodes occur predominantly over regions of lower rigidity. Modes with $q < (2n - 1)\pi$, on the other side of the n^{th} band gap, can be significantly stabilised since they are approximately 90° out-of-phase, and their antinodes sample a stiffer plate. The same argument applies for $q_* \lesssim (2n - 1)\pi$.

Our results suggest possible stability control strategies. By adding restoring forces (such as bending rigidity) with periodicity near the wavelength of the most unstable mode, stability can be enhanced or diminished at wavelengths either less than or greater than the band gap wavelength. Stabilisation of specific modes against Kelvin-Helmholtz instabilities can be achieved, but at the expense of destabilisation of other nearby modes.

Extensions of our approach to stability analysis in other fluid-structure systems should be possible. For example, the Orr-Sommerfeld problem (Orszag (1971)) in nonuniform Poiseuille flow through periodically elastic pipes can be similarly solved. A physical realization of flow through elastically periodic pipes may have arisen in the experiments of Krämer (1960) in which damping elements were periodically embedded along an elastic pipe. The Kelvin-Helmholtz type instability has been only briefly mentioned in this context by Benjamin (1960) and Landahl (1961), and only in uniform pipes. Moreover, the effects of periodicity on other classes of instabilities (*e.g.* Tollmien-Schlichting) have not been explored. It would also be interesting to consider the effects of dissipation, in both the fluid flow and the viscoelastic plate, on the stability properties of a periodic system.

The author was supported by the US National Science Foundation through grant DMS-0349195, and the US National Institutes of Health via grant K25AI058672.

REFERENCES

- ASHCROFT, N. W. & MERMIN, N. D. 1976 *Solid State Physics*. Thomson Learning, Inc.
- BENJAMIN, T. BROOKE 1960 Effects of a flexible boundary on hydrodynamic stability *J. Fluid Mech.* **9**, 513-533.
- BERMEL, P. A. & WARNER, M. 2002 Photonic band structure of cholesteric elastomers *Phys. Rev. E* **65**, 056614.

- BLANDFORD, R. D. & REES M. J. 1974 A 'twin-exhaust' model for double radio sources. *MNRAS*, **169**, 395-415.
- S. CHANDRASEKAR 1961 Hydrodynamic and Hydromagnetic Stability (Clarendon Press, Oxford)
- CHEN, L. S., KUO, C. H., YE, Z. & SUN, X. 2004 Band gaps in the propagation and scattering of surface water waves over cylindrical steps. *Phys. Rev. E* **69**, 066308.
- CHOU, T. 1998 Band structure of surface flexural-gravity waves along periodic interfaces. *J. Fluid Mech.* **369**, 333-350.
- DRAZIN, P. G. & REID, W. H. 2004 Hydrodynamic Stability (Cambridge University Press, Cambridge, UK).
- FRANK, A., JONES, T. W., RYU, D. & GAALAAS, J. B. 1996 The Magnetohydrodynamic Kelvin-Helmholtz Instability: A two-dimensional study. *Astrophysical J.* **460**, 777-793.
- HU, X. & CHAN, C. T. 2005 Refraction of Water Waves by Periodic Cylinder Arrays. *Phys. Rev. Lett.* **95**, 154501.
- HU, X., SHEN, Y., LIU, X., FU, R. AND ZI, J. 2003 Complete band gaps for liquid surface waves propagating over a periodically drilled bottom. *Phys. Rev. E* **68**, 066308.
- JOANNOPOULOS, J., MEADE, R. D., & WINN, J. N. 1995 *Photonic Crystals: Molding the Flow of Light*. Princeton University Press, Princeton, NJ.
- KRAMER, M. O. 1960 Boundary layer stabilization by distributed damping. *J. Amer. Soc. Nav. Engrs.* **72**, 25-33.
- LANDAHL, M. T. 1961 On the stability of a laminar incompressible boundary layer over a flexible surface *J. Fluid Mech.* **13**, 609-632.
- LINTON, C. M. & EVANS, D. V. 1990 The interaction of waves with arrays of vertical circular cylinders. *J. Fluid Mech.* **215**, 549-569.
- MILES, J. W. 1956 On the aerodynamic stability of thin panels *J. Aero. Sci.* **23**, 77.
- MILES, J. 2001 Stability of inviscid shear flow over a flexible boundary *J. Fluid Mech.* **434**, 371-378.
- NACIRI, M. & MEI, C. C. 1988 Bragg scattering of water waves by a doubly periodic seabed. *J. Fluid Mech.* **192**, 51-74.
- ORSZAG, S.A. 1971 Accurate Solution of the Orr Sommerfeld stability equation. *J. Fluid Mech.* **50**, 689-703.
- PETER, M. A., MEYLAN, M. H. & LINTON, C. M. 2006 Water-wave scattering by a periodic array of arbitrary bodies. *J. Fluid Mech.* **548**, 237-256.
- PORTER, R. & EVANS, D. V. 1996 Wave scattering by periodic arrays of breakwaters. *Wave Motion* **23**, 95-120.
- REISS, N. M. & CORONA, T. J. 1977 An Investigation of a Kelvin-Helmholtz Billow Cloud. *Bulletin of the American Meteorological Society* **58**, 159-162.
- SIGALAS, M. M. & ECONOMOU, E. N. 1992 Elastic and acoustic wave band structure. *J. Sound and Vibration* **158**, 377-382.
- WHITHAM, G. B. 1999 *Linear and Nonlinear Waves*. (Wiley Inter-Science).